0273-2289/06/129–132/621–630/$30.00

Modeling of a Continuous Pretreatment Reactor Using Computational Fluid Dynamics

R. Eric Berson,*,[1] Rajesh K. Dasari,[1] and Thomas R. Hanley[2]

[1]Department of Chemical Engineering, University of Louisville, Louisville, KY 40292, E-mail: eric.berson@ louisville.edu; and [2]Auburn University, Auburn, AL 36849

Abstract

Computational fluid dynamic simulations are employed to predict flow characteristics in a continuous auger driven reactor designed for the dilute acid pretreatment of biomass. Slurry containing a high concentration of biomass solids exhibits a high viscosity, which poses unique mixing issues within the reactor. The viscosity increases significantly with a small increase in solids concentration and also varies with temperature. A well-mixed slurry is desirable to evenly distribute acid on biomass, prevent buildup on the walls of the reactor, and provides an uniform final product. Simulations provide flow patterns obtained over a wide range of viscosities and pressure distributions, which may affect reaction rates. Results provide a tool for analyzing sources of inconsistencies in product quality and insight into future design and operating parameters.

Index Entries: Auger; biomass; CFD simulations; pretreatment reactor; screw conveyor.

Introduction

Methods such as acid pretreatments and enzymatic hydrolysis for converting biomass into high yields of pentose and hexose sugars to be used in fermentations are the subject of continuing investigations. Dilute acid hydrolysis, the most commonly used form of pretreatment, is a thermo-chemical process in which the biomass is in contact with a dilute acid, typically 2% or less sulfuric acid, at temperatures greater than 140°C for short residence times, usually on the order of 10 min or less *(1–5)*. The process produces hydrolysate liquor rich in pentose sugars and opens the ligno-cellulose pore structure to increase the susceptibility of cellulose to enzymatic attack *(6)*. Less than optimal processing conditions result in low sugar concentration and sugar degradation into substances toxic to a fermenting organism.

*Author to whom all correspondence and reprint requests should be addressed.

Other acid hydrolysis strategies are also presented in the literature: Nguyen et al. *(7)* recommended soaking in a 0.4–0.7 % sulfuric acid solution at 60°C for 4 h. Teixeira et al. *(8)* used a 60% solution of peracetic acid for 7 d. Choi and Matthews used a 2% solution of sulfuric acid at 132°C for 40 min followed by a 15% sulfuric acid solution at 132°C for 70 min *(9)*. Taherzadeh et al. *(10)* soaked different wood species in 5 g/L of sulfuric acid for 7 min between 188°C and 234°C *(10)*. Pretreatment at pilot or production scale must be performed as a continuous process to be economical. A number of successful continuous dilute acid processes have been reported *(7,11–16)*, but interest in processing at high solids concentrations has created unique processing challenges owing to high slurry viscosities. Screw augers are typically used for conveying viscous fluids but may not provide the optimal incorporation of acid and steam to produce a consistent pretreated biomass product. Over or under exposure of biomass to the acid, buildup on reactor walls, and poor heat transfer result from poor mixing and will lead to inconsistencies in the final product. Higher solids loading will provide more sugar yield if processed efficiently, but the increased viscosity may present a trade-off in terms of yield vs efficiency.

Berson and Hanley *(17)* presented flow patterns in screw auger pretreatment reactors created using computational fluid dynamics (CFD). Results showed distinct flow differences because of the auger design for a given viscosity. At solids loading in the 15–25% range, increasing the concentration of solids by 1% can increase the viscosity on the order of thousands of centipoise, significantly affecting flow conditions in the reactor. The objective of this study is to compare conditions in a screw auger pretreatment reactor for varying viscosities associated with varying solids loading and temperature using FLUENT 6.2, a commercial CFD flow simulation package. The reactor consists of a tubular shell around a screw auger used to convey the biomass slurry. Flow patterns and pressure distributions are revealed from simulations performed for slurries with solids concentrations ranging from 10% to 25%.

Materials and Methods

Biomass Slurry Preparation

Corn stover slurry pretreated with dilute sulfuric acid (190°C, 1.6% acid, 30% solids, 5 min residence time) was provided by the National Renewable Energy Laboratory. To prepare slurry for viscosity measurements, liquid hydrolysate and solids were separated by vacuum filtration. An appropriate amount of separated solids, containing 60% moisture after the filtration, were returned to the hydrolysate to obtain the desired solids concentration.

Viscosity Measurements

Biomass slurries containing suspended solids require a viscosity determination technique that maintains the solids in a uniform suspension

to prevent phase separation during measurement. A helical ribbon impeller fitted to Brookfield RVDV III (7187 dyne cm maximum torque) and HBDV III (57496 dyne cm maximum torque) rheometers is used to maintain particles in suspension for homogeneous viscosity determinations as suggested by Allen and Robinson *(18)*. This method assumes an average shear rate for the complex flow field created by the helical impeller that is proportional to the impeller speed:

$$\gamma_{avg} = k\mathrm{N} \tag{1}$$

and assumes the Reynolds number is inversely proportional to the dimensionless power number for Newtonian fluids in laminar flow:

$$c/\mathrm{Re} = \frac{2\pi M}{\rho N^2 D^5} \tag{2}$$

with:

$$\mathrm{Re} = \frac{\rho N D^2}{\eta}$$

where k and c are empirically determined constants. Solving for viscosity yields:

$$\eta = \frac{2\pi M}{cND^3} \tag{3}$$

or:

$$\eta = \frac{2\pi kM}{\gamma_{avg} cD^3} \tag{4}$$

Newtonian calibration fluids are used to calculate c in Eq. 3 using torque and rotational speed measurements from the viscometer. With a known value for c, k for the helical impeller is determined from Eq. 4. With known parameters, c and k, torque and rotational rate data from the helical fitted viscometer can be used to determine biomass slurry viscosities.

CFD Modeling

The Gambit 1.6 preprocessor is used for creating a geometric rendering representing the flow domain in the reactor with the domain divided into 261,773 tetrahedral shaped discrete control volumes that comprise the computational grid. Solutions are obtained with the FLUENT 6.2 solver, a commercial CFD software package that models fluid flow in any geometry. The solver employs a finite-volume discretization process to numerically solve the governing equations for conservation of mass and momentum. Algebraic equations are constructed from the governing differential equations and integrated into each control volume. The equations are linearized and

Table 1
Viscosity as a Function of Solids Concentration
(25°C, $\gamma = 1/s$)

Solids (%)	Viscosity (cP)
10	680
15	16,000
17	28,600
25	41,700

a solution of the equation system gives updated values for the dependent variables, such as velocities, pressures, and so on. The general form of the mass conservation equation is written as:

$$\frac{\partial \rho}{\partial t} + \nabla \cdot (\rho V) = S_m \tag{5}$$

and the momentum conservation equation is written as:

$$\frac{\partial}{\partial t}(\rho V) + \nabla \cdot (\rho V V) = -\nabla P + \rho g + \nabla(\eta \nabla V) \tag{6}$$

that includes terms to account for pressure, gravitational, and viscous forces.

The reactor dimensions are 1.52 m in length and 0.15 m in diameter. A screw shaft along the length of the reactor rotates at 5 rpm. Material enters at one of the horizontal reactor and for a boundary condition, the pressure at the exit is assumed to be atmospheric. Gravitational forces are neglected. All simulations are performed using the laminar flow model: Reynolds numbers ranged between 5.6 at 1000 cP and 112.5 at 20,000 cP. Motion of the shaft is generated with the rotating reference frame model that provides a steady state solution and is commonly used to model flow in rotating equipment *(19)*.

Results and Discussion

Table 1 shows a significant increase in viscosity for a given temperature, in this case 25°C, as the concentration of biomass solids increases from 10% to 25%. The increase is particularly significant in the 10% through 17% range in which an increase of 1% solids results in an average increase of 4000 cP. Above 17%, the consistency becomes closer to a wet solid rather than a suspension of particles. Viscosity still increases considerably with a small increase in solids between 17% and 25%, but the average increase drops to 1600 cP per 1% increase in solids.

If the material is heated to the reactor's typical operating temperature, 190°C, evaporation of the liquid will result in inaccurate viscosity measurements. Instead, viscosities were measured at temperatures from

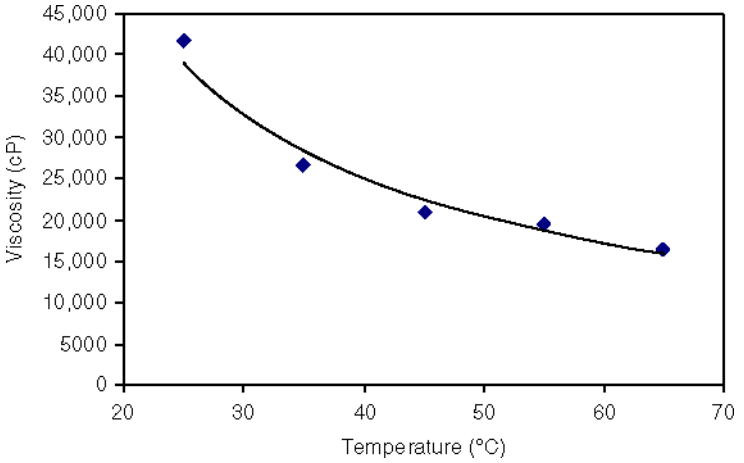

Fig. 1. Viscosity as a function of temperature (25% solids, $\gamma = 1/s$).

Fig. 2. Reactor shaft with location of cross-sectional plane.

25°C to 65°C, the maximum temperature before liquid losses begin to affect torque measurements by the viscometer. It is inadvisable to extrapolate viscosity to 190°C and, fortunately, not necessary since the decrease in viscosity begins to level off by 65°C. Figure 1 shows the viscosity–temperature relationship for 25% solids concentration between 25°C and 65°C. The viscosity decreases from 41,700 cP at 25°C to less than 20,000 cP at 65°C. The consistency of the lowest solids concentration considered here, 10%, is much thinner, and temperature has less effect on viscosity. Torque at 25°C, corresponding to a viscosity of 680 cP, is less than 3% of the viscometer's maximum. At this low range, the viscometer did not register differences in torque measurements for different temperatures.

Based on viscosity–temperature data for 10% and 25% solids, viscosities = 1000, 5000, 10,000, and 20,000 cP were chosen for simulations to compare flow characteristics over this range of concentrations. Because the actual viscosity is not known at 190°C, the four viscosities do not correlate directly to specific solids concentrations and temperatures, but are chosen

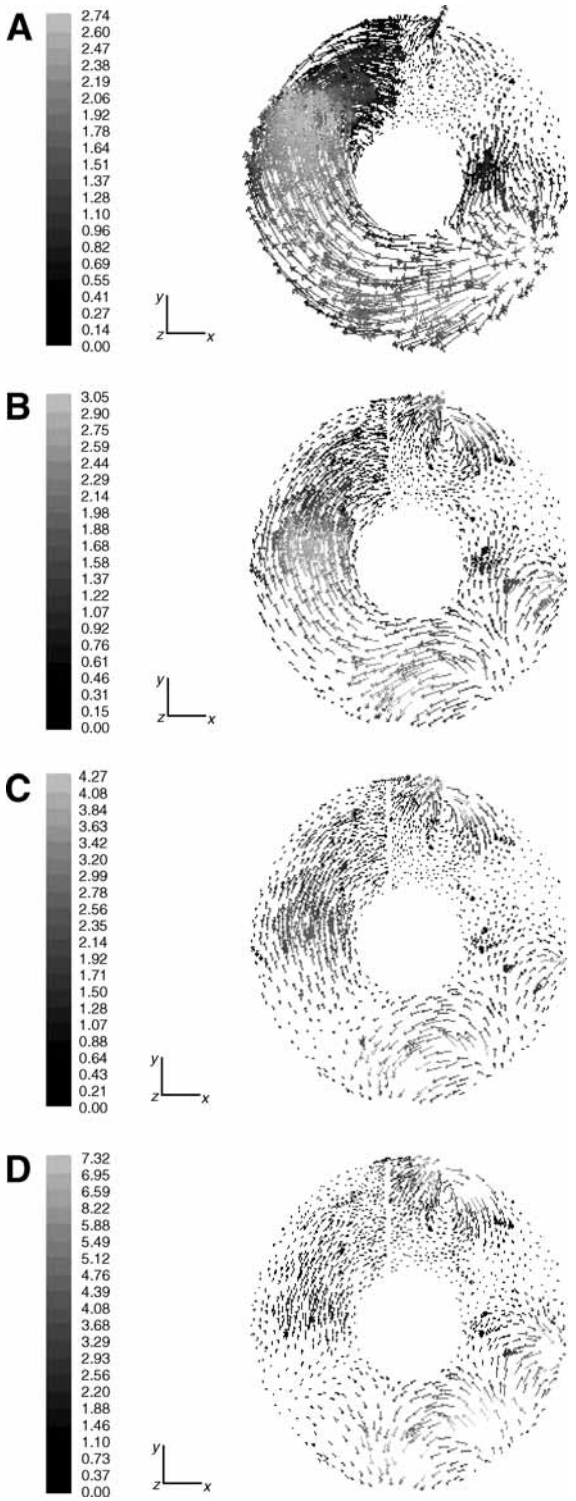

Fig. 3. Velocity vectors in a cross-sectional mixing plane (scale in m/s). **(A)** 1000 cP b, **(B)** 5000 cP, **(C)** 10,000 cP, **(D)** 20,000 cP.

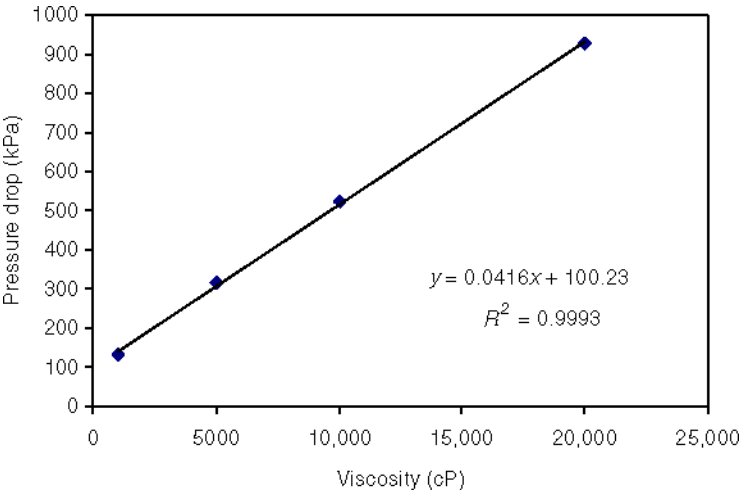

Fig. 4. Pressure drop across reactor as a function of viscosity.

to provide a qualitative comparison covering the approximate range of viscosities that likely exists within the reactor.

Velocity vectors provide a qualitative means of comparing flow characteristics between the four cases. Figure 2 shows the location of a cross-sectional plane 1 m from in which the material enters the reactor. In Fig. 3A through 3D, a perpendicular view shows vectors in this plane for each of the four cases. At the lowest viscosity, a more organized circular pattern is observed (Fig. 3A). As the viscosity increases, the velocity vectors become less pronounced in the tangential direction as the rotation of the shaft has less of a rotational impact on fluid away from the surface of each screw flight. The greater flow resistance exhibited at higher viscosities results in less tangential and more axial flow between screw flights.

The spiraling nature of the fluid movement, as it circulates while proceeding axially, is evident at any viscosity as some areas within a plane contain longer tangential vectors, and some areas contain smaller vectors that appear as dots, indicating motion perpendicular to the plane. The flow patterns indicate better mixing is likely occurring at lower viscosities, which is expected, because there is more tangential motion in addition to the axial motion. However, the higher viscosity fluids do exhibit some localized regions of high intensity circulation that provides some mixing benefits.

Higher solids loading is desirable to help reduce the size of production scale reactors, but these results indicate a trade-off may be necessary if poor mixing at higher viscosities results in inconsistencies in the final product stream. Even if the solids are soaked in the liquid phase before entering the reactor, good mixing is still needed for a uniform temperature distribution. The inclusion of vertical baffles located between screw flights should significantly enhance mixing.

Pressure drop appears to vary linearly with viscosity (Fig. 4). Poiseuille's equation,

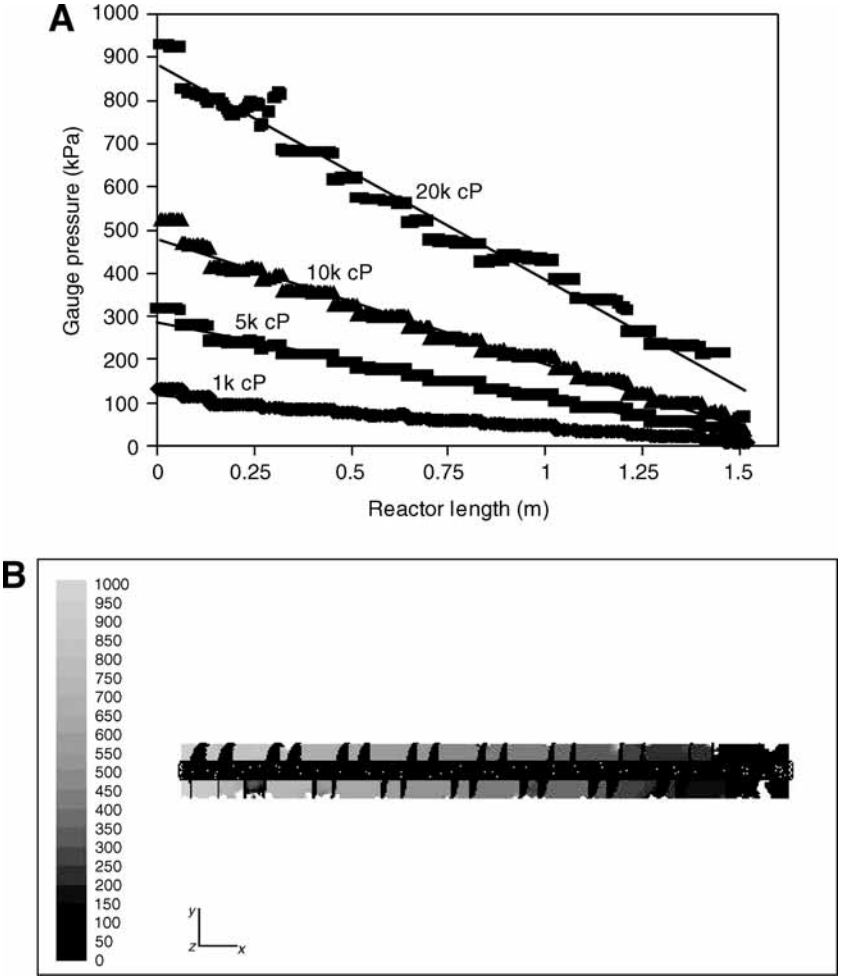

Fig. 5. Pressure distribution along length of reactor. **(A)** Pressure distribution along length of reactor (linear regressions, 1k cP = 0.971, 5k cP = 0.980, 10k cP = 0.982, 20k cP = 0.975). **(B)** Contours of pressure distribution along length of reactor (20k cP).

$$\Delta P = \frac{F8\eta L}{\pi r^4} \tag{7}$$

predicts this for laminar flow in a straight pipe, but interestingly, this relationship is valid even with the flow altered owing to the rotating shaft. Although the relationship applies at this slow rotation rate, 5 rpm, it is uncertain if it will apply at higher rotation rates having different flow characteristics.

The pressure drop across the length of the reactor increases about sevenfold as the viscosity increases from 1000 cP to 20,000 cP. Figure 5A shows total pressure distribution along the length of the reactor for each of the four cases. Higher pressure may result in higher hydrolysis

reaction rates that can have adverse implications regarding sugar degradation into toxic byproducts. The 132 kPa pressure drop for a 1000 cP fluid provides a more uniform pressure distribution throughout the length of the reactor, and likely more uniform local reaction rates, compared with the higher viscosity fluids were the pressure drop is as high as 927 kPa for a 20,000 cP fluid.

Pressure appears to vary linearly with reactor length, which is also predicted by Poiseuille's equation. The data segments that appear to "stair-step" in Fig. 5A coincide with the shaded pressure contours in between consecutive screw flights in Fig. 5B (only 20k cP case is shown), with each segment beginning and ending at a screw flight.

Conclusions

Viscosity increases by approx 4000 cP for each 1% increase in solids concentration between 10% and 17%, and by approx 1600 cP for each 1% increase between 17% and 25%. The tangential component of flow is more pronounced at lower viscosities, indicating the likelihood of increased contact between the dilute acid liquid and biomass solids. Pressure drop increases linearly with viscosity, and is seven times that for 20,000 cP than for 1000 cP. Results provide a tool for analyzing sources of inconsistencies in product quality and insight into future design and operating parameters.

Acknowledgment

This work was funded by the US Department of Energy's National Renewable Energy Laboratory, subcontract: XCO-1-31016-01.

Nomenclature

c	Newtonian proportionality constant (dimensionless)
D	Diameter (m)
F	Volumetric flow rate (m^3/s)
k	Shear rate constant (dimensionless)
L	Length (m)
M	Torque (Nm)
N	Rotation rate (rps)
P	Pressure (Pa)
r	Radius (m)
Re	Reynolds number (dimensionless)
V	Velocity (m/s)
γ	Shear rate (/s)
η	Viscosity (kg/m·s)
ρ	Density (kg/m^3)

References

1 Schell, D. J., Walter, P. J., and Johnson, D. K. (1992), *Appl. Biochem. Biotechnol.* **34–35,** 659–665.
2 Schell, D. J., Farmer, J., Newman, M., and McMillan, J. D. (2003), *Appl. Biochem. Biotechnol.* **105–108,** 69–85.
3 Zhu, Y., Lee, Y. Y., and Elander, R. T. (2005), *Appl. Biochem. Biotechnol.* **121–124,** 1045–1054.
4 Torget, R. W., Walter, P. J., Himmel, M., and Grohmann, K. (1991), *Appl. Biochem. Biotechnol.* **28–29**, 75–86.
5 Wang, S. S. and Converse, A. O. (1992), *Appl. Biochem. Biotechnol.* **34–35**, 61–75.
6 McMillan, J. D. (1997), *Renewable Energy* **10(2/3)**, 295–302.
7 Nguyen, Q. A., Keller, F. A., Tucker, M. P., et al. (1999), *Appl. Biochem. Biotechnol.* **77–79**, 455–472.
8 Teixeira, L. C., Linden, J. C., and Schroeder, H. A. (1999), *Appl. Biochem. Biotechnol.* **77–79**, 19–34.
9 Choi, C. H. and Matthews, A. P. (1996), *Bioresour. Technol.* **58(2),** 101–106.
10 Taherzadeh, M. J., Elkund, R., Gustafsson, L., Nicklasson, C., and Liden, G. (1997), *Ind. Eng. Chem. Res.* **36(11),** 4659–4665.
11 Tucker, M. P., Farmer, J. D., Keller, F. A., Schell, D. J., and Nguyen, Q. A. (1998), *Appl. Biochem. Biotechnol.* **70–72**, 25–35.
12 Nguyen, Q. A., Tucker, M. P., Keller, F. A., and Eddy, F. P. (2000), *Appl. Biochem. Biotechnol.* **84–86**, 561–576.
13 Torget, R. W., Hayward, T. K., and Elander, R. (1997), presented at the *19th Symposium on Biotechnology for Fuels and Chemicals*, Colorado Springs, CO.
14 Chen, R., Wu, Z., and Lee, Y. Y. (1998), *Appl. Biochem. Biotechnol.* **70–72**, 37–49.
15 Lee, Y. Y., Wu, Z., and Torget, R. W. (2000), *Bioresour. Technol.* **71**, 29–39.
16 Converse, A. O. (2002), *Bioresour. Technol.* **81**, 109–116.
17 Berson, R. E. and Hanley, T. R. (2005), *Appl. Biochem. Biotechnol.* **121–124,** 935–945.
18 Allen, D. G. and Robinson, C. W. (1990), *Chem. Eng. Sci.* **45(1)**, 37–48.
19 Fluent, Inc. (2003) FLUENT 6.1 User's Guide, Fluent, Inc., Lebanon, NH.